Brain Imaging and Behavior
https://doi.org/10.1007/s11682-017-9816-6

ORIGINAL RESEARCH

Functional brain abnormalities in major depressive disorder using the Hilbert-Huang transform

Haibin Yu[1] · Feng Li[2] · Tong Wu[1] · Rui Li[3] · Li Yao[1,4] · Chuanyue Wang[2] · Xia Wu[1,4]

Abstract

Major depressive disorder is a common disease worldwide, which is characterized by significant and persistent depression. Non-invasive accessory diagnosis of depression can be performed by resting-state functional magnetic resonance imaging (rs-fMRI). However, the fMRI signal may not satisfy linearity and stationarity. The Hilbert-Huang transform (HHT) is an adaptive time–frequency localization analysis method suitable for nonlinear and non-stationary signals. The objective of this study was to apply the HHT to rs-fMRI to find the abnormal brain areas of patients with depression. A total of 35 patients with depression and 37 healthy controls were subjected to rs-fMRI. The HHT was performed to extract the Hilbert-weighted mean frequency of the rs-fMRI signals, and multivariate receiver operating characteristic analysis was applied to find the abnormal brain regions with high sensitivity and specificity. We observed differences in Hilbert-weighted mean frequency between the patients and healthy controls mainly in the right hippocampus, right parahippocampal gyrus, left amygdala, and left and right caudate nucleus. Subsequently, the above-mentioned regions were included in the results obtained from the compared region homogeneity and the fractional amplitude of low frequency fluctuation method. We found brain regions with differences in the Hilbert-weighted mean frequency, and examined their sensitivity and specificity, which suggested a potential neuroimaging biomarker to distinguish between patients with depression and healthy controls. We further clarified the pathophysiological abnormality of these regions for the population with major depressive disorder.

Keywords Depression · Resting-state functional magnetic resonance imaging · Hilbert-Huang transform · Hilbert-weighted mean frequency · Multivariate receiver operating characteristic analysis

Introduction

Major depressive disorder (MDD) is a commonly occurring mental disease characterized by persistent depressed mood, cognitive impairments, anhedonia, and thinking retardation (Zeng et al. 2012; Otte et al. 2016; McIntyre et al. 2016). The current diagnosis of MDD is largely dependent on self-reported symptoms and clinical signs (Wu et al. 2011; Young et al. 2016). However, the variety of clinical manifestations may affect the accuracy of the diagnosis (Yao et al. 2009). Neuroimaging techniques such as magnetic resonance imaging (MRI), positron emission tomography (PET), and electroencephalogram (EEG) can provide a direct, non-invasive, and reliable approach for the assessment of structural, physiological, and biochemical features of the brain (Ferenci et al. 2002). Thus, neuroimaging technique may promote more accurate clinical diagnosis and further understanding of the pathophysiology of depression.

Resting-state functional MRI (rs-fMRI) is a frequently used neuroimaging tool to investigate MDD (Bluhm et al. 2009; Chen et al. 2012; Guo et al. 2012; Kenny et al. 2010; Zhou et al. 2010). The rs-fMRI can contribute to a more in-depth exploration of the neural mechanisms of MDD, because the spontaneous brain activity in the resting state may be related to the internal process of self-presentation

✉ Xia Wu
wuxia@bnu.edu.cn

1 College of Information Science and Technology, Beijing Normal University, No. 19 Xin Jie Kou Wai Da Jie, Beijing 100875, China

2 Beijing Key Laboratory for Mental Disorders, Center of Schizophrenia, Beijing Institute for Brain Disorders, Beijing Anding Hospital of Capital Medical University, Beijing 10088, China

3 CAS Key Laboratory of Mental Health, Institute of Psychology, Beijing 100101, China

4 State Key Laboratory of Cognitive Neuroscience and Learning & IDG/McGovern Institute for Brain Research, Beijing Normal University, Beijing 100875, China

Published online: 09 February 2018

disunited from the environment (Liu et al. 2014). Furthermore, the rs-fMRI is relatively simple, because the only requirement for the participant is to remain stationary (Liu et al. 2013). To extract the features of interest from rs-fMRI signals, time-domain methods are frequently used. These have been used to determine the temporal correlation between fMRI signals using functional connectivity (FC) and region homogeneity (ReHo) methods. For example, studies have demonstrated that patients with depression have a decreased functional connection coefficient of the cortical and limbic system, and a tendency of decreased connectivity between the anterior cingulate cortex (ACC) and amygdala (Anand et al. 2005). These previous findings support the hypothesis that imbalances in cortico-limbic activity and connectivity may underlie the pathophysiology of MDD. Furthermore, Liu et al. (2010) reported a decreased regional homogeneity in the insula and cerebellum in MDD, while Yao et al. (2009) demonstrated that patients with MDD had a ReHo decrease mainly in the frontal and limbic lobes as well as the basal ganglia during resting state, which may be useful as biomarkers for the diagnosis of MDD.

Frequency-domain methods, such as the amplitude of low frequency fluctuation (ALFF; Zang et al. 2007) and fractional ALFF (fALFF; Zou et al. 2008), have also been used to extract features of rs-fMRI signals. Both ALFF and fALFF can provide information on low-frequency signal activity, which is complementary to the previously mentioned time-domain methods (Yang et al. 2007; Zang et al. 2007; Zou et al. 2008). Previous studies have reported increased ALFF in the frontal cortex, basal ganglia, left insular cortex, right anterior entorhinal cortex, and left inferior parietal cortex, along with decreased ALFF in the bilateral occipital cortex, cerebellum hemisphere, and right superior temporal cortex of patients with MDD, which may be associated with cognitive control deficits in emotional processing in these patients (Liu et al. 2014). Furthermore, patients with MDD showed increased fALFF in the right dorsal medial frontal gyrus, which suggests a critical role of this brain region in depressive symptomatology (Liu et al. 2013). However, those frequency-domain methods are usually based on the unrealistic assumption that the system represented by the blood-oxygen-level dependent (BOLD) method is linear and stationary.

The time-domain methods generally suffer from less sparse and poor data representation, while the frequency-domain methods have poor temporal resolution (Martis et al. 2012). To overcome these limitations, a number of results have been proposed recently. These suggested that the time–frequency method can reflect the change of amplitude with time and provide information on the fluctuation signals in the frequency domain (Mezer et al. 2009). Wavelet transforms (Bullmore et al. 2004; Van De Ville et al. 2006) have been used on Parkinson's fMRI data to detect differences in network efficiency between patients and healthy participants (Skidmore et al. 2011). Furthermore, short-time Fourier transform has been used by Mezer et al. (2009) to characterize the time dependency of frequency changes in rs-fMRI time series and achieve good clustering. Nevertheless, these methods are limited by the inherent assumptions of the signal, namely the linearity and stationarity for the short-time Fourier analysis and linearity for the Wavelet analysis, while these hypotheses have not been validated in the fMRI time series (Lange and Zeger 1997; Van Someren 2011; Song et al. 2014; Qian et al. 2015). In addition, due to the limitation of the uncertainty principle (Robertson 1929), most of the traditional time–frequency methods are limited in providing both high temporal resolution and high frequency resolution at the same time.

The Hilbert-Huang transform (HHT; Huang et al. 1998) is an adaptive time–frequency analysis method, which is suitable for nonlinear and non-stationary signals (Qian et al. 2015). The HHT has a good time–space and frequency-space resolution and can facilitate precise expressions of instantaneous frequency, which is conducive to feature extraction of biomedical signals (Huang 2014; Huang and Wu 2008; Donnelly 2006; Peng et al. 2005; Huang et al. 2008). The HHT mainly consists of two parts, namely the empirical mode decomposition (EMD; Huang and Shen 2005) and the Hilbert transformation. The EMD is an efficient and adaptive method to extract a set of intrinsic mode functions (IMFs) from nonlinear and non-stationary time series (Lin and Zhu 2012), which was first proposed by Huang et al. (1998). Recently, both HHT and EMD have been widely used in rs-fMRI. Previous studies have adopted EMD and its improved method to decompose the rs-fMRI time series of each voxel into several components with distinct frequency bands in order to analyze the frequency specific to the resting-state brain activity (Qian et al. 2015, 2017; Song et al. 2014). Furthermore, Qian et al. (2017) applied an improved EMD method to the study of brain network in resting state in Parkinson's disease and comorbid depression. Their results demonstrated that these decomposed characteristic oscillatory activities may contribute to distinct motor and non-motor components of clinical injuries in Parkinson's disease. Therefore, we hypothesized that HHT and EMD could also find more biological information in MDD.

In this article, we applied HHT to study the abnormal information of rs-fMRI in patients with MDD. Previous studies have shown that MDD often involves abnormalities in specific neuroanatomic circuits, e.g., the prefrontal-amygdalar-pallidostriatal-mediothamic mood regulating circuit (MRC; Anand et al. 2005, 2007), and the limbic-cortical-striatal-pallidal-thalamic circuit (LCSPT; Sheline 2000, 2003). Therefore, we combined the data from multiple brain regions to obtain features with higher distinction accuracy. Our analysis showed that the Hilbert-weighted mean

frequency (HWMF) differences between the MDD group and healthy controls (HC) are mainly observed in the right hippocampus, right parahippocampal gyrus, left amygdala, and left and right caudate nucleus. To cross-validate these findings, we applied both ReHo and fALFF methods on the same datasets. Our results showed that the HHT requires only 27 distinct brain regions to distinguish between MDD and HC, whereas ReHo and fALFF require 41 and 36 brain regions, respectively. Thus, the proposed analysis framework is useful in establishing quantitative indicators for the clinical diagnosis of depression, and can better assist the clinical diagnosis and effective evaluation in MDD.

Methods and materials

Participants

In this study, two classes of participants were examined: (i) patients who had already been diagnosed with MDD (n = 35), and (ii) healthy controls matched by age, sex, and education level (n = 37). All participants were right-handed. Patients with MDD were recruited from the Anding Hospital, Capital Medical University, while the healthy controls were recruited through newspaper advertisements. The clinical states of the patients were measured by the 17-item Hamilton Depression Rating Scale (HAMD; Hamilton 1967) and the Hamilton anxiety scale (HAMA). The following patients were included in the study: (1) aged 18–65 years, with the ability to give voluntary informed consent; (2) meeting the Diagnostic and Statistical Manual of Mental Disorders-4th edition (DSM-IV) criteria for Major Depressive Episode and having an HAMD score ≥ 17; (3) satisfying the criteria to undergo MRI scan based on an MRI screening questionnaire; and (4) able to be managed as outpatients. We excluded patients who (1) met the DSM-IV criteria for schizophrenia, schizoaffective disorder, obsessive–compulsive disorder, or an anxiety disorder as a primary diagnosis; (2) had any serious unstable illnesses requiring medications or hospitalization, including hepatic, renal, gastroenterologic, respiratory, cardiovascular (including ischemic heart disease), endocrinologic, neurologic, immunologic, or hematologic disease; (3) had a history of head trauma resulting in loss of consciousness; (4) were aged less than 18 years or more than 65 years; (5) were left handed; (6) displayed evidence of being an imminent danger to self or others; or (7) were pregnant, breast-feeding, or had other contraindications to MRI at the time of the study. The HC were interviewed using the Structured Clinical Interview for DSM-IV, non-patient edition, to confirm the absence of any history of psychiatric or neurologic illness. Exclusion criteria of the HC included those who had a first-degree relative with any mental illness or a second-degree family member with a psychotic disorder or who have not satisfied the criteria of MRI scanning. Our study was approved by the Institutional Review Board of Anding Hospital, Capital Medical University and Imaging Center for Brain Research, State Key Laboratory of Cognitive Neuroscience and Learning, Beijing Normal University. After reading a description of the study procedures, all participants signed an informed consent form. The basic characteristics of both patients with MDD and HC including the distribution of sex, age, duration of disease, and other indicators were summarized in Table 1.

The MRI data acquisition

The rs-fMRI data used in this study were collected on a 3.0-Tesla scanner (Siemens, Erlangen, Germany) at the National Key Laboratory for Cognitive Neuroscience and Learning, Beijing Normal University, and a single-shot T2* weighted gradient *echo-planar imaging* (PEI) sequence was used. The parameters' settings were as follows: *repetition time* (TR) = 2,000 ms, *echo time* (TE) = 30 ms, *flip angle* (FA) = 90 degrees, *matrix size* = 64 × 64, *field of view* (FOV) = 220 mm × 220 mm, total 240 volumes, *slice thickness* = 3.5 mm, *skip* = 0.6 mm, and *slices number* = 33. In this data acquisition process, all participants were instructed to keep their heads fixed, eyes closed, and stay awake, without doing any physical and mental activities.

Image preprocessing

Considering the scanner calibration and participants' adaption to the lab station, the first 10 time-series points of each rs-fMRI scan were removed, and the remaining functional images were transformed from DICOM to NIFTI format using the MRIcron software (http://www.mricro.com).

Table 1 Demographic information and disease severity in the two groups

Variables (Mean ± SD)	MDD (n = 35)	HC (n = 37)	p-value
Age (year)	36 ± 13.80	36.3 ± 13.28	0.92[a]
Sex (Female/Male)	17/17	16/21	0.66[b]
HAMD	21.57 ± 4.48	0	5.05E-41[a]
HAMA	20.25 ± 7.07	0.19 ± 0.46	7.25E-27[a]
Education level (year)	13.75 ± 3.01	12.93 ± 2.40	0.61[a]
Age range	18–65	19–60	--
Illness Duration (year)	6.99 ± 8.83	--	--

HAMA Hamilton Anxiety Scale, *HAMD* Hamilton Depression Rating Scale (17-item scale), *HC* healthy controls, *MDD* major depressive disorder, *SD* standard deviation

[a]Two-sample *t*-test, [b]Chi-square two-tailed test

The software SPM8 (http://www.fil.ion.ucl.ac.uk/spm) was used for slice timing, head motion correction, and normalization by using EPI templates. The above-mentioned steps depended on the following parameters: *number of slices* = 33, *voxels of the normalized images* = 3 × 3 × 3 mm^3; no translation or rotation movement in any data set exceeded ± 2 mm or ± 2°. The linear trend was removed to reduce the impact of device instability. After these steps, the AAL template was used to define the 90 regions of interest (ROIs) for each participant (Tzourio 2002). Subsequently, the ROI time course was extracted by calculating the average time series of all voxels in one ROI.

The EMD and HWMF

The HHT was used to analyze the preprocessed ROI time series further in order to extract the corresponding time–frequency features. The process mainly included three steps. First, the EMD method (Huang and Shen 2005) was applied on the ROI time series and a finite set of intrinsic oscillatory components, known as IMFs (Huang 2014; Huang and Wu 2008; Ding et al. 2007) was extracted. Second, for each IMF, the Hilbert transform was performed to obtain the analytical transformation of the input signal. The signal's instantaneous amplitude and phase were calculated according to the analytic transformation. Finally, the Hilbert-weighted frequency of each IMF (Xie and Wang 2006) and the Hilbert-weighted mean frequency (HWMF) of the original signal (Song et al. 2015) were calculated.

Empirical mode decomposition

The EMD is an important part of the HHT method, which can extract a series of IMFs from nonlinear and non-stationary biomedical signals step by step with good efficiency and adaptability (Lin and Zhu 2012). In order to ensure that a meaningful instantaneous frequency (e.g., no negative value) can be obtained by HHT, all IMFs need to satisfy the following two conditions: (i) the upper envelope and the lower envelope must have symmetry, i.e., the mean value of the upper and lower envelopes defined by local maxima and local minima is always zero at all points; and (ii) the number of extrema and the number of zero crossings must either be equal or differ at most by one. Through the standard EMD algorithm depicted in Huang et al. (1998), the fMRI time series were divided into a set of IMFs and the remaining residual according to the following equation:

$$x(t) = \sum_{i=1}^{N} IMF_i(t) + r(t) \tag{1}$$

where N is the number of intrinsic mode functions.

The standard EMD algorithm was performed as follows:

1. Find all the local extrema of the input signal *x(t)*.
2. Interpolate all the local minima to generate the lower envelope *elow(t)* and all the local maxima to generate the upper envelope *eup(t)*.
3. Compute the local mean time course *emean(t)* based on the following equation:

$$emean(t) = \left[elow(t) + eup(t)\right]/2 \tag{2}$$

4. Obtain the "oscillatory-mode" *r(t)* using the following formula:

$$r(t) = x(t) - emean(t) \tag{3}$$

5. If *r(t)* obeys the two criteria of the IMF, then $IMF_i = r(t)$ becomes an IMF; If *r(t)* is monotonic, the application completes; otherwise set $x(t) = r(t)$ and then repeat the process from Step 1.

Hilbert-weighted mean frequency

The Hilbert transform can describe the local properties of the signal (Peng et al. 2005). After the decomposition step, the Hilbert transform was performed for each IMF to obtain the instantaneous information about amplitude and phase. The specific algorithm was calculated as follows:

1. For each IMF we obtained after the EMD algorithm, Hilbert transform was applied according to the following formula:

$$y_i = \frac{P}{\pi}\int_{-\infty}^{+\infty} \frac{IMF_i(\tau)}{t-\tau} d\tau \tag{4}$$

where *P* is the Cauchy principal value.

2. Construct a complex signal $z_i(t)$ to obtain the instantaneous frequency:

$$z_i(t) = IMF_i(t) + iy_i(t) = a_i(t)e^{i\theta_i(t)} \tag{5}$$

$$a_i(t) = \sqrt{IMF_i^2(t) + y_i^2(t)} \tag{6}$$

$$\theta_i(t) = \arctan\left(\frac{y_i(t)}{IMF_i(t)}\right) \tag{7}$$

where $ai(t)$ represents the instantaneous amplitude, and $\theta_i(t)$ represents the instantaneous phase.

3. The instantaneous frequency of each IMF was defined as follows:

$$\omega_{\mathrm{i}}(\mathrm{t}) = \frac{d\theta_i(t)}{dt} \tag{8}$$

4. The Hilbert-weighted frequency can reflect the mean oscillation frequency of the IMF, and can be obtained by the following formula:

$$\mathrm{HWF_i} = \frac{\sum_{j=1}^{m} \omega_i(j) a_i^2(j)}{\sum_{j=1}^{m} a_i^2(j)} \tag{9}$$

5. The HWMF of the input signal was defined as follows:

$$\mathrm{HWMF} = \frac{\sum_{\mathrm{i=1}}^{\mathrm{N}} \|\mathrm{a_i}\| \mathrm{HWF_i}}{\sum_{\mathrm{i=1}}^{\mathrm{N}} \|\mathrm{a_i}\|} \tag{10}$$

It is worth mentioning that, biologically, HWMF represents the velocity of the original BOLD oscillation (Song et al. 2015). The HWMF, i.e., the overall frequency of the original fMRI time series of the voxel, takes the contributions of all the IMFs into consideration and assumes that the IMFs with higher energy will contribute more to the mean frequency (Song et al. 2015).

Multivariate receiver operating characteristic (ROC) analysis based on logistic regression

The multivariate ROC method is a composite of a various-variable model (logistic regression) and a single-variable model (the ROC curve analysis) (Copas and Corbett 2002; Pepe et al. 2006). The former was used for the analysis of single or multiple covariates and generating variables containing prediction probabilities, and the latter used the predictive values generated by the logistic regression as *test variable*, which were the initial analysis variables for the ROC curve. In medical research, the multivariate ROC method can be used to predict the probability of a disease according to risk factors (Hosmer and Lemesbow 1980), while the ROC analysis is an ideal and classical method for analyzing and evaluating the diagnostic accuracy of biomarkers, and is widely used to reflect the sensitivity and specificity of biomarkers in examing disease (Fawcett 2006; Obuchowski 2003). The detailed steps of our multivariate ROC method were as follows:

1) Two-sample *t*-test was performed on HWMF in each of the 90 brain regions of patients and controls. Subsequently, all groups of HWMF were sorted according to the p-values. The ROC analysis was used to analyze the HWMF corresponding to the brain region with the smallest p-value in the diseased and non-diseased populations, and the area under ROC curve (AUC) was recorded.
2) Two sets of variables with the smallest p-values were used as initial variables. By means of the logistic regression model, a linear transformation was applied to these independent variables to generate new variables containing individual prediction probabilities for achieving the purpose of dimensionality reduction.
3) Subsequently, the ROC analysis was performed using the new variables as *test variable*.

The AUC is a summary measure of accuracy, which is the most extensive diagnostic accuracy index for diagnostic tests with continuous diagnostic or ordinal data (Begg 1991; Pepe and Thompson 2000; El et al. 2009). The AUC ranges from 0.5 to 1, with *1* representing perfect discrimination and *0.5* representing no discrimination capacity. If the AUC was not 1, the next set of data with the minimal p-value was added to our independent variables, and steps 2 and 3 were subsequently repeated. Otherwise, the application completes. The whole calculation process of this method was realized using IBM SPSS Statistics 20.

Comparative analysis based on ReHo and fALFF

In order to verify the validity of the HHT method, we adopted ReHo and fALFF from the common time-based and frequency-based methods for comparative analysis. Kendall's coefficient of concordance (KCC) is often used to measure the similarity or synchrony of the time courses (Tononi et al. 1998) and is the most commonly selected feature of the ReHo method (Guo et al. 2011; Qiu et al. 2011; Wu et al. 2011). In addition, the fALFF value is the basic feature extracted by the fALFF method (Liu et al. 2013; Zang et al. 2007; Zou et al. 2008). Therefore, ReHo and fALFF methods were applied to the same dataset as the HHT method, and the same multivariate ROC method was used to the extracted KCC and fALFF values.

Results

The results of the HHT method

As shown in Fig. 1, after EMD, the data for each ROI of each participant was decomposed into six IMFs and one residual. The chart indicates that the first IMF has the highest frequency bands, the last IMF has the lowest frequency bands, and the other IMFs are in the middle. The Hilbert transform is subsequently applied on each IMF and the instantaneous frequency is calculated.

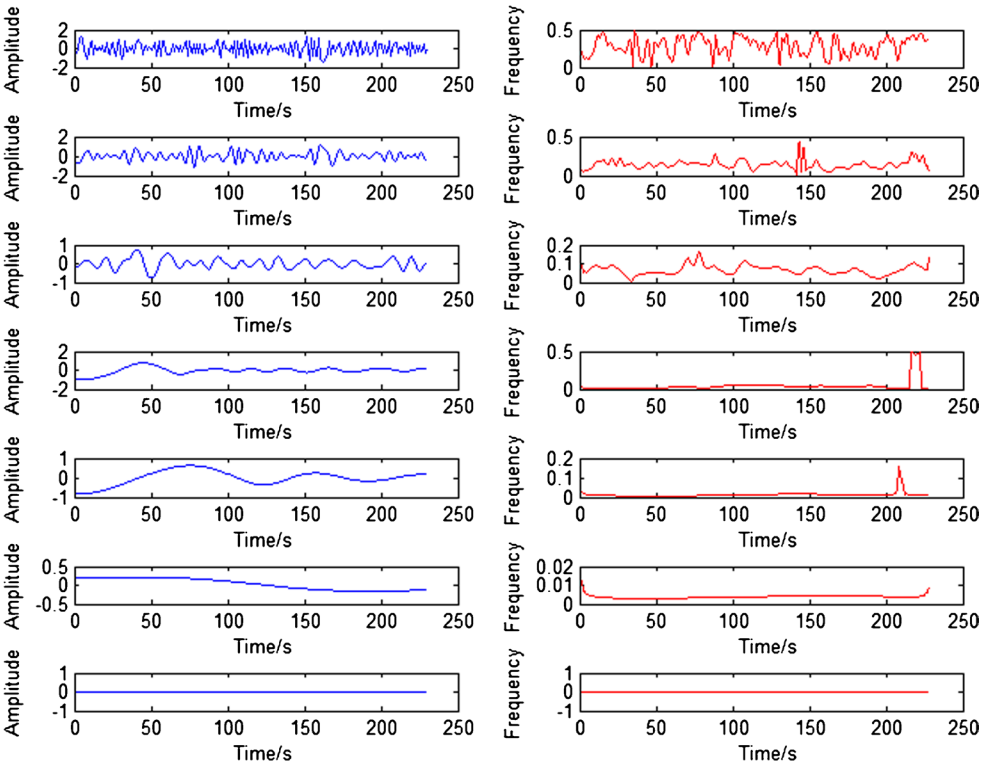

Fig. 1 One example of intrinsic mode functions (IMFs) (blue) and instantaneous frequency (red) for one dataset. The left represents one example of the decomposed IMFs (blue), the horizontal axis represents the time points, and the vertical axis represents the amplitude of the decomposed signals, the right represents the calculated instantaneous frequency of each major IMF using Hilbert transform (red), the horizontal axis represents the time points, and the vertical axis represents the instantaneous frequency. The IMF order gradually increased from top to bottom, and the amplitude and instantaneous frequency gradually reduced

Different brain regions obtained through HHT

On the basis of the calculated HWMF of the 90 brain regions of the 72 participants, we selected 27 possible brain regions that could distinguish the HC and MDD groups by the multivariate ROC curve. As shown in Fig. 2, when multivariate ROC analysis was applied to the HWMF of the following 27 brain regions, the AUC reached the value of 1, which means that these characteristics have a good distinction between healthy participants and patients with depression (Zweig and Campbell 1993). These 27 brain regions, arranged in ascending order of p-values, are the left caudate nucleus, right middle frontal gyrus, left thalamus, left anterior cingulate and paracingulate gyri, left inferior occipital gyrus, right caudate nucleus, left lenticular nucleus, putamen, left middle frontal gyrus, right middle frontal gyrus, orbital part, right lenticular nucleus, pallidum, right temporal pole: middle temporal gyrus, left cuneus, right olfactory cortex, right middle temporal gyrus, right superior frontal gyrus, medial orbital, right inferior parietal, but supramarginal and angular gyri, right inferior frontal gyrus, opercular part, right insula, left supramarginal gyrus, left amygdala, right superior temporal gyrus, right thalamus, left olfactory cortex, left calcarine fissure and surrounding cortex, right heschl gyrus, right parahippocampal gyrus, right hippocampus. (Figs. 2, 3).

Different brain regions obtained through ReHo and fALFF

On the basis of the calculated KCC of the 90 brain regions of the 72 participants, 41 possible brain regions were selected to distinguish the HC from the MDD group with the multivariate ROC curve. As shown in Fig. 4, when multivariate ROC analysis was applied to the KCC of the following 41 brain regions, the AUC reached the value of 1. These 41 brain regions, arranged in ascending order of p-values are the right thalamus, left inferior temporal gyrus, left hippocampus, left inferior occipital gyrus, left fusiform gyrus, left lenticular nucleus, putamen, left thalamus, right caudate nucleus, right precentral gyrus, left precentral gyrus, right inferior occipital gyrus, left postcentral gyrus, left caudate nucleus, left lingual gyrus, right hippocampus, right postcentral gyrus, right lenticular nucleus, putamen, left calcarine fissure and surrounding cortex, left rolandic operculum, right lingual gyrus, left heschl gyrus, left insula, left middle occipital gyrus, left middle temporal gyrus, left superior temporal gyrus, right inferior temporal gyrus, right anterior cingulate and paracingulate gyri, left median cingulate and paracingulate gyri, right fusiform gyrus, right heschl gyrus, left inferior frontal gyrus, opercular part, right superior temporal gyrus, left inferior parietal, but supramarginal and angular gyri, right inferior frontal gyrus, opercular part, right inferior frontal gyrus, triangular part, right

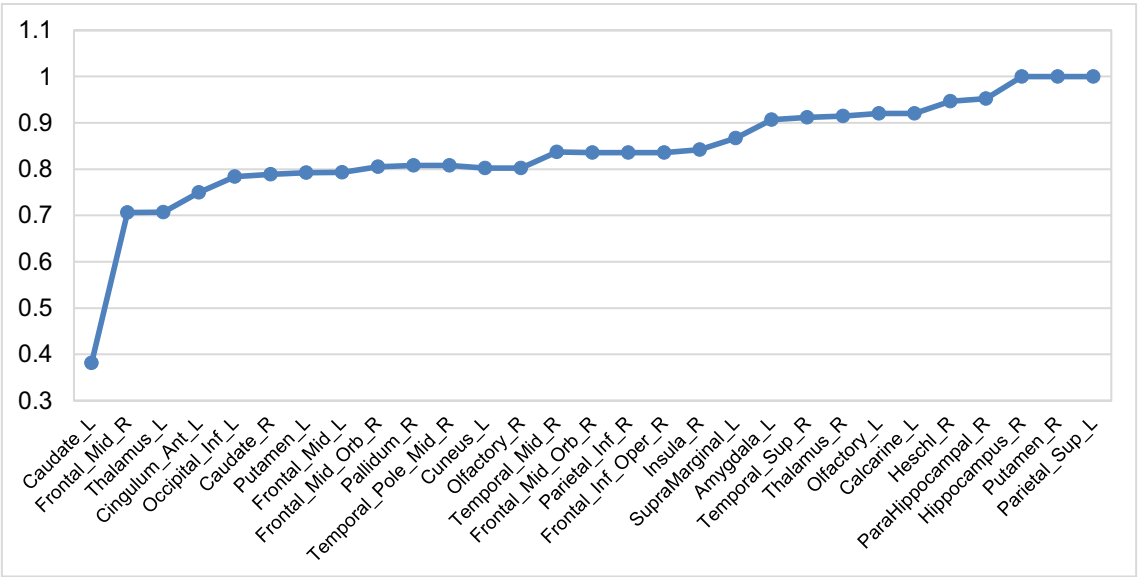

Fig. 2 Area under the curve (AUC) shows an increase with regions of interest (ROIs) arranged in increasing order of p values, based on Hilbert-weighted mean frequency (HWMF). The horizontal axis represents the 27 abnormal ROIs arranged in ascending order of p-value; the vertical axis represents the AUC value. The 27 abnormal brain regions obtained by our Hilbert-Huang transform method are the left caudate nucleus, right middle frontal gyrus, left thalamus, left anterior cingulate and paracingulate gyri, left inferior occipital gyrus, right caudate nucleus, left lenticular nucleus, putamen, left middle frontal gyrus, right middle frontal gyrus, orbital part, right lenticular nucleus, pallidum, right temporal pole: middle temporal gyrus, left cuneus, right olfactory cortex, right middle temporal gyrus, right superior frontal gyrus, medial orbital, right inferior parietal, but supramarginal and angular gyri, right inferior frontal gyrus, opercular part, right insula, left supramarginal gyrus, left amygdala, right superior temporal gyrus, right thalamus, left olfactory cortex, left calcarine fissure and surrounding cortex, right heschl gyrus, right parahippocampal gyrus, right hippocampus

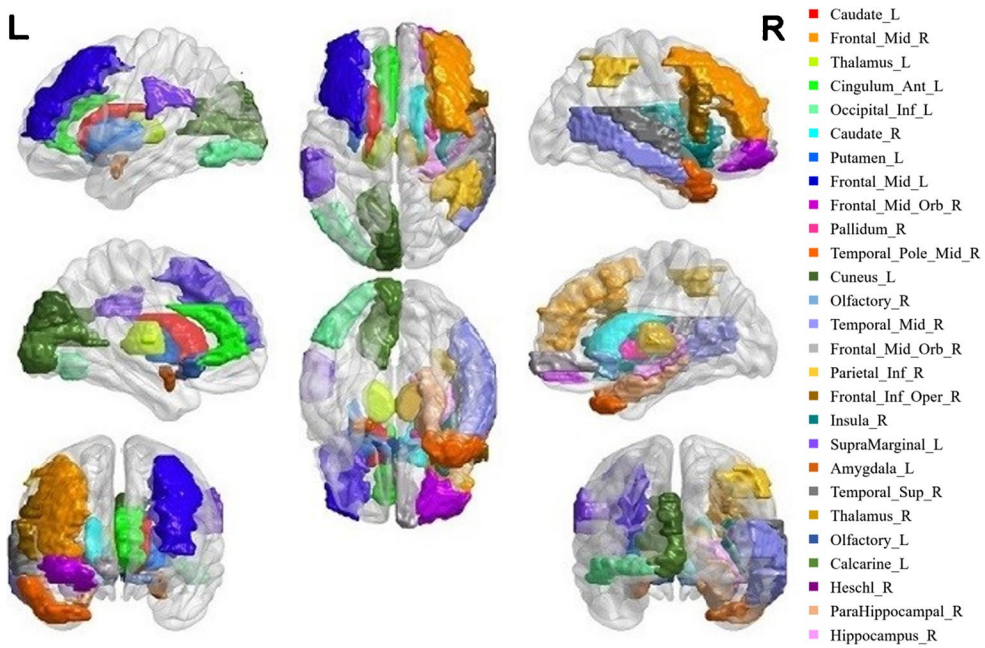

Fig. 3 The whole brain mapping of 27 different brain regions. The 27 abnormal brain regions arranged in ascending order of p-value are the left caudate nucleus, right middle frontal gyrus, left thalamus, left anterior cingulate and paracingulate gyri, left inferior occipital gyrus, right caudate nucleus, left lenticular nucleus, putamen, left middle frontal gyrus, right middle frontal gyrus, orbital part, right lenticular nucleus, pallidum, right temporal pole: middle temporal gyrus, left cuneus, right olfactory cortex, right middle temporal gyrus, right superior frontal gyrus, medial orbital, right inferior parietal, but supramarginal and angular gyri, right inferior frontal gyrus, opercular part, right insula, left supramarginal gyrus, left amygdala, right superior temporal gyrus, right thalamus, left olfactory cortex, left calcarine fissure and surrounding cortex, right heschl gyrus, right parahippocampal gyrus, right hippocampus

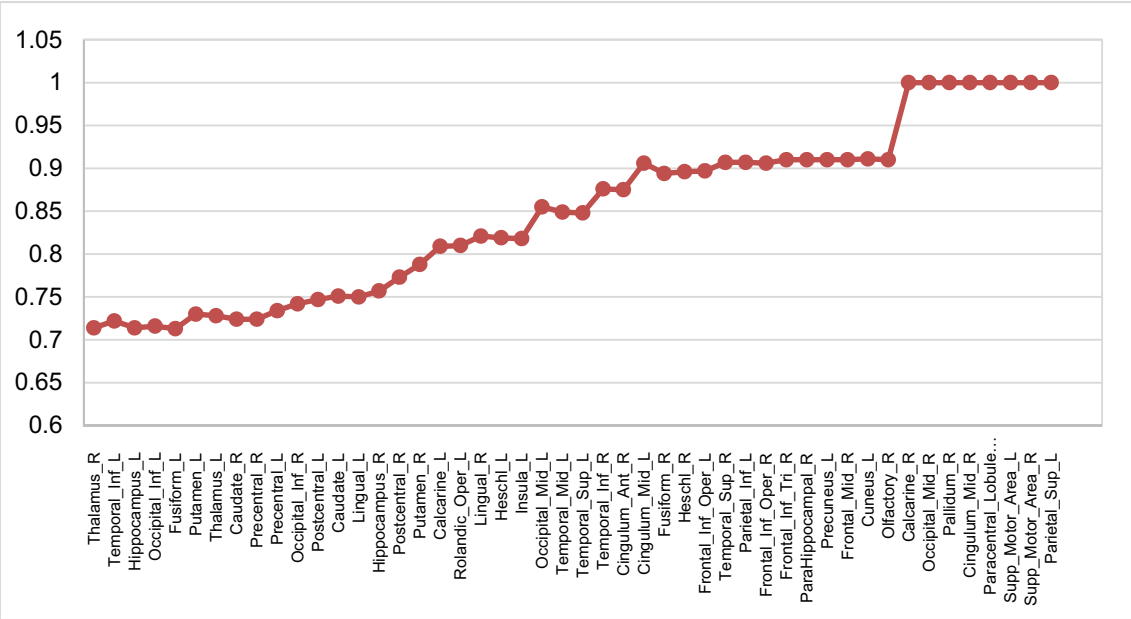

Fig. 4 Area under the curve (AUC) shows an increase with regions of interest (ROIs) arranged in increasing order of p values based on Kendall's coefficient of concordance (KCC). The 41 abnormal ROIs are arranged in ascending order of p-value on the horizontal axis; the vertical axis represents the AUC value. The 41 abnormal brain regions obtained by the region homogeneity (ReHo) method are the right thalamus, left inferior temporal gyrus, left hippocampus, left inferior occipital gyrus, left fusiform gyrus, left lenticular nucleus, putamen, left thalamus, right caudate nucleus, right precentral gyrus, left precentral gyrus, right inferior occipital gyrus, left postcentral gyrus, left caudate nucleus, left lingual gyrus, right hippocampus, right postcentral gyrus, right lenticular nucleus, putamen, left calcarine fissure and surrounding cortex, left rolandic operculum, right lingual gyrus, left heschl gyrus, left insula, left middle occipital gyrus, left middle temporal gyrus, left superior temporal gyrus, right inferior temporal gyrus, right anterior cingulate and paracingulate gyri, left median cingulate and paracingulate gyri, right fusiform gyrus, right heschl gyrus, left inferior frontal gyrus, opercular part, right superior temporal gyrus, left inferior parietal, but supramarginal and angular gyri, right inferior frontal gyrus, opercular part, right inferior frontal gyrus, triangular part, right parahippocampal gyrus, left precuneus, right middle frontal gyrus, left cuneus, right olfactory cortex, right calcarine fissure and surrounding cortex

parahippocampal gyrus, left precuneus, right middle frontal gyrus, left cuneus, right olfactory cortex, right calcarine fissure and surrounding cortex.

On the basis of the calculated fALFF of the 90 brain regions of the 72 participants, we selected 36 possible brain regions that could distinguish the HC from the MDD group with the multivariate ROC curve. As shown in Fig. 5, when multivariate ROC analysis was applied to the fALFF of the following 36 brain regions, the AUC reached the value of 1. These 36 brain regions, arranged in ascending order of p-values, are the left thalamus, right thalamus, right inferior occipital gyrus, left lenticular nucleus, putamen, left inferior occipital gyrus, right lenticular nucleus, pallidum, right caudate nucleus, left fusiform gyrus, right lingual gyrus, right fusiform gyrus, left caudate nucleus, right heschl gyrus, right calcarine fissure and surrounding cortex, left calcarine fissure and surrounding cortex, left precentral gyrus, left postcentral gyrus, left lenticular nucleus, pallidum, right hippocampus, right precentral gyrus, right lenticular nucleus, putamen, left lingual gyrus, left hippocampus, left inferior temporal gyrus, left middle occipital gyrus, left heschl gyrus, right inferior temporal gyrus, right postcentral gyrus, right middle occipital gyrus, left rolandic operculum, right parahippocampal gyrus, right superior occipital gyrus, left superior temporal gyrus, right gyrus rectus, right olfactory cortex, right cuneus, left insula.

Comparison of the HHT, ReHo, and fALFF methods

In order to verify the validity of the HHT method, which is a time–frequency analysis method, we chose ReHo and fALFF from the common time-based methods and frequency-based methods for comparative analysis. We selected the KCC and fALFF values as the calculated features through ReHo and fALFF. As shown in Fig. 6, when the value of AUC was 1, the number of brain regions required by HWMF was 27, compared with 41 and 36 brain regions required by the KCC and fALFF, respectively.

Discussion

To determine a more comprehensive and accurate biomarker that reflects the pathophysiological abnormalities of depression, we used the HHT method on the rs-fMRI data from patients with depression and healthy controls

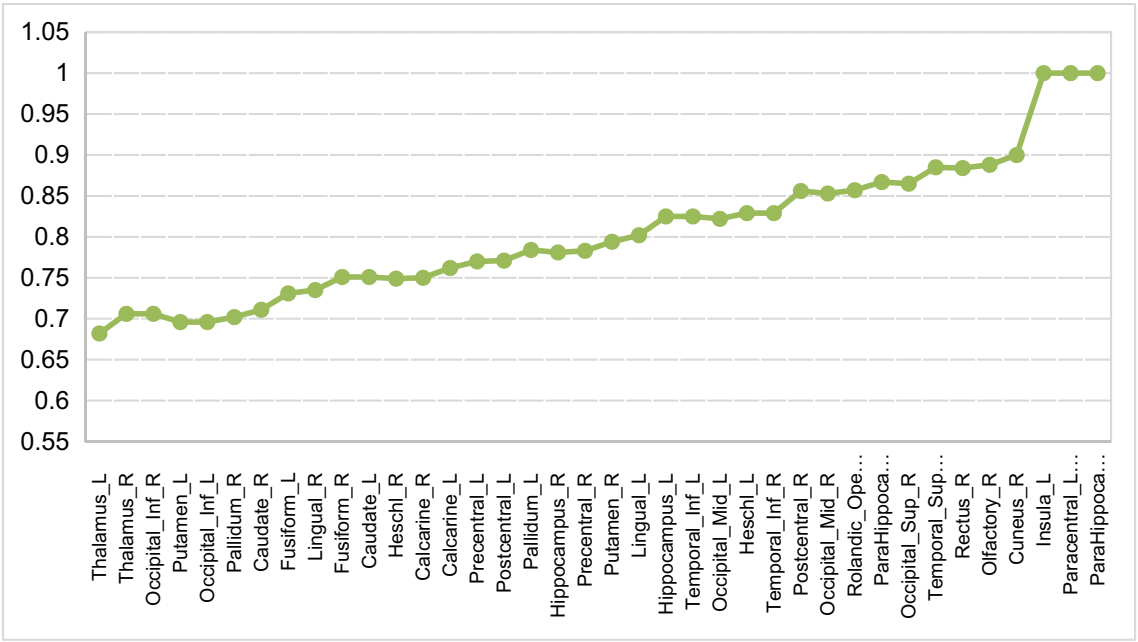

Fig. 5 Area under the curve (AUC) shows an increase with regions of interest (ROIs) arranged in increasing order of p values based on fractional amplitude of low frequency fluctuation (fALFF). The horizontal axis represents the 36 abnormal ROIs arranged in ascending order of p-value; the vertical axis represents the AUC value. The 36 abnormal brain regions obtained by the fALFF method are the left thalamus, right thalamus, right inferior occipital gyrus, left lenticular nucleus, putamen, left inferior occipital gyrus, right lenticular nucleus, pallidum, right caudate nucleus, left fusiform gyrus, right lingual gyrus, right fusiform gyrus, left caudate nucleus, right heschl gyrus, right calcarine fissure and surrounding cortex, left calcarine fissure and surrounding cortex, left precentral gyrus, left postcentral gyrus, left lenticular nucleus, pallidum, right hippocampus, right precentral gyrus, right lenticular nucleus, putamen, left lingual gyrus, left hippocampus, left inferior temporal gyrus, left middle occipital gyrus, left heschl gyrus, right inferior temporal gyrus, right postcentral gyrus, right middle occipital gyrus, left rolandic operculum, right parahippocampal gyrus, right superior occipital gyrus, left superior temporal gyrus, right gyrus rectus, right olfactory cortex, right cuneus, left insula

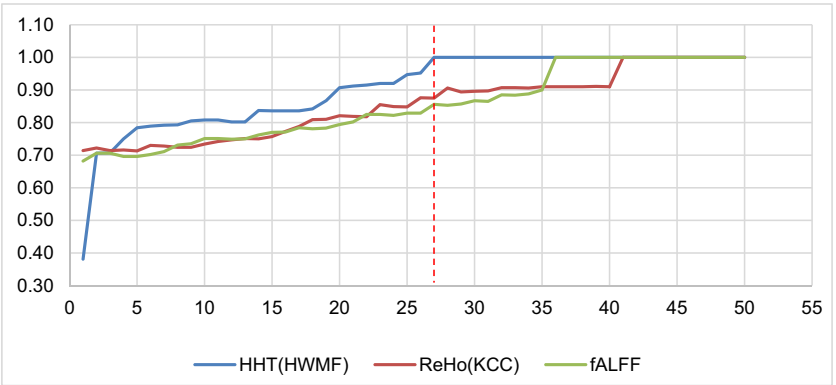

Fig. 6 Comparison of area under the curve (AUC) trends of the three methods. The horizontal axis represents the number of brain regions; the vertical axis represents the AUC value. The lines are colored in blue, red, and green indicating HHT (HWMF), ReHo (KCC), and fALFF (fALFF), respectively. The red vertical dotted line corresponding to the abscissa value is 27

and analyzed the HWMF of multiple brain regions with the multivariate ROC method. The hippocampus is a part of the brain's limbic system and is mainly responsible for learning and memory. In our findings, the AUC value increased from 0.947 to 1, and the distinction efficiency reached 100% after adding the HWMF of the right hippocampus and right parahippocampal gyrus. Similarly, our analysis based on the ReHo and fALFF methods also yielded the right hippocampus and right parahippocampal gyrus. Numerous studies have reported that hippocampal volume reductions are likely to be associated with depression (Kim et al. 2008; Sheline 2011; Malykhin and Coupland 2015). Furthermore, Finkelmeyer et al. (2016) demonstrated that patients with MDD had hippocampal functional abnormalities that were independent of the structural abnormalities (i.e., volumetric reductions). The amygdala also belongs to the limbic system, and is related to human emotion, learning, and memory. Thus,

when the HWMF of the left amygdala was added into our analysis, the AUC increased, as should be expected, from 0.867 to 0.907. Furthermore, Mah (2007) and Drevets et al. (2002) have reported that amygdala abnormalities were also associated with depression. Recent studies also indicated that the functional and structural abnormalities of the hippocampus and amygdala were strongly consistent in patients with MDD (Rigucci et al. 2010; Kempton et al. 2011; Murray et al. 2011; Tahmasian et al. 2013). In addition to the hippocampus and amygdala, the thalamus is also included in the limbic-thalamic-cortical. Based on our results, both the left and right thalamus were included in the differential brain areas obtained by the HHT, ReHo, and fALFF methods. Anand et al. (2005) have reported that abnormal brain regions in patients with depression were mainly concentrated in the limbic system, including the thalamus and the ACC. It has been shown that the ACC plays the role of a bridge between the processing of attention and emotion (Bush et al. 2000; Devinsky et al. 1995). Neuroimaging studies have also demonstrated that functional and structural ACC abnormalities accompany MDD (Drevets et al. 2008; Hamilton et al. 2013). Moreover, Anand et al. (2009) have reported that depression may be associated with the ACC and thalamic circulation.

The other arm of the LCSPT circuit is the cortico-striatal-pallidal-thalamic (CSPT) branch, which mainly consists of the caudate, putamen, and globus pallidus (pallidum). Our analysis showed that the HWMF of the caudate nucleus on both sides contributed greatly to the increase of the AUC value; the KCC and fALFF values of the caudate nucleus also had the same effect. It has been previously reported that depression may be associated with functional or structural abnormalities in the caudate nucleus (Kim et al. 2008; Krishnan et al. 1992; Pizzagalli et al. 2009). The caudate putamen and the nucleus of the putamen, which form the new striatum, are important components of the basal ganglia. Anomalies in the structure and function of the striatum, such as altered regional blood flow (Videbech 2000) and glucose metabolism (Dunn et al. 2002) have been previously reported. The globus pallidus also belongs to a part of the loop. As may be expected, both the left putamen and right pallidum made significant contributions to the increase of the AUC value in our HHT-based analysis. We observed a similar trend with the addition of the left putamen and the right pallidum in the analysis based on the ReHo and fALFF methods. Furman et al. (2011) demonstrated aberrant connectivity in the frontal lobes and striatum (which consists of the caudate nucleus, putamen, and core of the nucleus accumbens), thus providing strong evidence that the CSPT is associated with depression. Previous studies have shown that MDD may be associated with the LCSPT circuit (Liu et al. 2010; Sheline 2003), which is in line with our present results. In particular, we have found that 27 brain regions with significant differences were associated with this loop.

In order to verify the validity of the HHT method, which belongs to time–frequency analysis methods, we chose ReHo and fALFF from the common time-based and frequency-based methods for comparative analysis. When the value of AUC was 1 (Fig. 6), the number of brain regions required by the HWMF was 27, whereas that required for KCC and fALFF was 41 and 36, respectively. On the other hand, when the number of brain regions is 27, the AUC values corresponding to the HHT, ReHo, and fALFF methods are 1, 0.875, and 0.856, respectively (Fig. 6). Thus, compared with ReHo and fALFF, HWMF extracted by HHT contained more time–frequency information, at least in the datasets used in this present study.

In the current study, we applied the HHT method to MDD patients and identified a potential neuroimaging biomarker to distinguish them from healthy controls. Nevertheless, this study has several limitations that are worth noting. Firstly, from the present results, the statistical potency of the given small samples is of potential significance. Further studies need to be conducted on a larger cohort. Moreover, other neuroimaging evidence such as structural abnormalities can also be combined with the present results to establish a comprehensive biological marker in order to obtain a more reliable clinical diagnosis of depression. Further research will be conducted in our next study.

Conclusion

The rs-fMRI signals can be used as reliable indicators of mental diseases such as depression. Traditional time-based methods, frequency-based methods, or time–frequency based methods are limited in reflecting the information comprehensively or providing high temporal and frequency resolutions simultaneously. Therefore, we applied the HHT method in the present study. Considering that multiple brain areas may reflect deeper information, we conducted a joint analysis of multiple brain regions, by applying multivariate ROC analysis to distinguish effectively healthy from depression samples. The AUC of the selected features of 27 brain regions reached the value of 1, and these features could effectively distinguish patients with depression form healthy controls. These results contributed to the establishment of quantitative indicators for the clinical diagnosis of depression and could better assist the clinical diagnosis of depression and effective evaluation.

Acknowledgements The authors gratefully acknowledge Beijing Normal University Imaging Center for Brain Research for the contributions in MRI data acquisition.

Funding This work was supported by the Funds for the general Program of the National Natural Science Foundation of China (61571047, 81471389), Beijing Science and Technology Commission (D121100005012002), Beijing Municipal Administration of Hospitals Clinical Medicine Development of Special Funding Support (ZYLX201403) and CAS Key Laboratory of Mental Health, Institute of Psychology (KLMH2015G06).

Compliance with Ethical Standards

Conflict of interest The authors declare that they have no conflict of interest.

Ethical approval All procedures performed in studies involving human participants were in accordance with the ethical standards of the institutional and/or national research committee and with the 1964 Helsinki declaration and its later amendments or comparable ethical standards.

Informed consent Informed consent was obtained from all individual participants included in the study.

References

Anand, A., Li, Y., Wang, Y., Gardner, K., & Lowe, M. J. (2007). Reciprocal effects of antidepressant treatment on activity and connectivity of the mood regulating circuit: an FMRI study. *The Journal of Neuropsychiatry and Clinical Neurosciences, 19*(3), 274–282.

Anand, A., Li, Y., Wang, Y., Lowe, M. J., & Dzemidzic, M. (2009). Resting state corticolimbic connectivity abnormalities in unmedicated bipolar disorder and unipolar depression. *Psychiatry Research: Neuroimaging, 171*(3), 189–198.

Anand, A., Li, Y., Wang, Y., Wu, J., Gao, S., Bukhari, L., … & Lowe, M. J. (2005). Activity and connectivity of brain mood regulating circuit in depression: a functional magnetic resonance study. *Biological Psychiatry, 57*(10), 1079–1088.

Anand, A., Li, Y., Wang, Y., Wu, J., Gao, S., Bukhari, L., … & Lowe, M. J. (2005). Antidepressant effect on connectivity of the mood-regulating circuit: an FMRI study. *Neuropsychopharmacology, 30*(7), 1334.

Begg, C. B. (1991). Advances in statistical methodology for diagnostic medecine ni the 1980's. *Statistics in Medicine, 10*(12), 1887–1895.

Bluhm, R., Williamson, P., Lanius, R., Théberge, J., Densmore, M., Bartha, R., … & Osuch, E. (2009). Resting state default-mode network connectivity in early depression using a seed region-of-interest analysis: decreased connectivity with caudate nucleus. *Psychiatry and Clinical Neurosciences, 63*(6), 754–761.

Bullmore, E., Fadili, J., Maxim, V., Şendur, L., Whitcher, B., Suckling, J., … & Breakspear, M. (2004). Wavelets and functional magnetic resonance imaging of the human brain. *Neuroimage, 23*, S234-S249.

Bush, G., Luu, P., & Posner, M. I. (2000). Cognitive and emotional influences in anterior cingulate cortex. *Trends in Cognitive Sciences, 4*(6), 215–222.

Chen, J. D., Liu, F., Xun, G. L., Chen, H. F., Hu, M. R., Guo, X. F., … & Zhao, J. P. (2012). Early and late onset, first-episode, treatment-naive depression: same clinical symptoms, different regional neural activities. *Journal of Affective Disorders, 143*(1), 56–63.

Copas, J. B., & Corbett, P. (2002). Overestimation of the receiver operating characteristic curve for logistic regression. *Biometrika, 89*(2), 315–331.

Devinsky, O., Morrell, M. J., & Vogt, B. A. (1995). Contributions of anterior cingulate cortex to behaviour. *Brain, 118*(1), 279–306.

Ding, H., Huang, Z., Song, Z., & Yan, Y. (2007). Hilbert–Huang transform based signal analysis for the characterization of gas–liquid two-phase flow. *Flow Measurement and Instrumentation, 18*(1), 37–46.

Donnelly, D. (2006). The fast Fourier and Hilbert-Huang transforms: a comparison. Computational Engineering in Systems Applications, IMACS Multiconference on (Vol. 1, pp. 84–88). IEEE.

Drevets, W. C., Bogers, W., & Raichle, M. E. (2002). Functional anatomical correlates of antidepressant drug treatment assessed using PET measures of regional glucose metabolism. *European Neuropsychopharmacology, 12*(6), 527–544.

Drevets, W. C., Price, J. L., & Furey, M. L. (2008). Brain structural and functional abnormalities in mood disorders: implications for neurocircuitry models of depression. *Brain Structure and Function, 213*(1–2), 93–118.

Dunn, R. T., Kimbrell, T. A., Ketter, T. A., Frye, M. A., Willis, M. W., Luckenbaugh, D. A., & Post, R. M. (2002). Principal components of the Beck Depression Inventory and regional cerebral metabolism in unipolar and bipolar depression. *Biological Psychiatry, 51*(5), 387–399.

El Khouli, R. H., Macura, K. J., Barker, P. B., Habba, M. R., Jacobs, M. A., & Bluemke, D. A. (2009). Relationship of temporal resolution to diagnostic performance for dynamic contrast enhanced MRI of the breast. *Journal of Magnetic Resonance Imaging, 30*(5), 999–1004.

Fawcett, T. (2006). An introduction to ROC analysis. *Pattern Recognition Letters, 27*(8), 861–874.

Ferenci, P., Lockwood, A., Mullen, K., Tarter, R., Weissenborn, K., & Blei, A. T. (2002). Hepatic encephalopathy—definition, nomenclature, diagnosis, and quantification: final report of the working party at the 11th World Congresses of Gastroenterology, Vienna, 1998. Hepatology, 35(3), 716–721.

Finkelmeyer, A., Nilsson, J., He, J., Stevens, L., Maller, J. J., Moss, R. A., … & McAllister-Williams, R. H. (2016). Altered hippocampal function in major depression despite intact structure and resting perfusion. *Psychological Medicine, 46*(10), 2157–2168.

Furman, D. J., Hamilton, J. P., & Gotlib, I. H. (2011). Frontostriatal functional connectivity in major depressive disorder. *Biology of Mood & Anxiety Disorders, 1*(1), 11.

Guo, W. B., Liu, F., Chen, J. D., Gao, K., Xue, Z. M., Xu, X. J., … & Chen, H. F. (2012). Abnormal neural activity of brain regions in treatment-resistant and treatment-sensitive major depressive disorder: a resting-state fMRI study. *Journal of Psychiatric Research, 46*(10), 1366–1373.

Guo, W. B., Sun, X. L., Liu, L., Xu, Q., Wu, R. R., Liu, Z. N., … & Zhao, J. P. (2011). Disrupted regional homogeneity in treatment-resistant depression: a resting-state fMRI study. *Progress in Neuro-Psychopharmacology and Biological Psychiatry, 35*(5), 1297–1302.

Hamilton, J. P., Chen, M. C., & Gotlib, I. H. (2013). Neural systems approaches to understanding major depressive disorder: an intrinsic functional organization perspective. *Neurobiology of Disease, 52*, 4–11.

Hamilton, M. A. X. (1967). Development of a rating scale for primary depressive illness. *British Journal of Clinical Psychology, 6*(4), 278–296.

Hosmer, D. W., & Lemesbow, S. (1980). Goodness of fit tests for the multiple logistic regression model. *Communications in Statistics-Theory and Methods, 9*(10), 1043–1069.

Huang, H., & Pan, J. (2006). Speech pitch determination based on Hilbert-Huang transform. *Signal Processing, 86*(4), 792–803.

Huang, M., Wu, P., Liu, Y., Bi, L., & Chen, H. (2008). Application and contrast in brain-computer interface Between hilbert-huang transform and wavelet transform. In *Young Computer Scientists, 2008.*

ICYCS 2008. The 9th International Conference for (pp. 1706–1710). IEEE.

Huang, N. E. (2014). Hilbert-Huang transform and its applications (Vol. 16). World Scientific.

Huang, N. E., & Shen, S. S. P. (2005). *Hilbert-Huang Transform and Its Applications*. Singapore: World Scientific. https://doi.org/10.1142/5862.

Huang, N. E., Shen, Z., Long, S. R., Wu, M. C., Shih, H. H., Zheng, Q., … & Liu, H. H. (1998). The empirical mode decomposition and the Hilbert spectrum for nonlinear and non-stationary time series analysis. *In Proceedings of the Royal Society of London A: Mathematical, Physical and Engineering Sciences*, 454(1971), 903–995. The Royal Society.

Huang, N. E., & Wu, Z. (2008). A review on Hilbert-Huang transform: Method and its applications to geophysical studies. *Reviews of Geophysics*, 46(2).

Kempton, M. J., Salvador, Z., Munafò, M. R., Geddes, J. R., Simmons, A., Frangou, S., & Williams, S. C. (2011). Structural neuroimaging studies in major depressive disorder: meta-analysis and comparison with bipolar disorder. *Archives of General Psychiatry, 68*(7), 675–690.

Kenny, E. R., O'Brien, J. T., Cousins, D. A., Richardson, J., Thomas, A. J., Firbank, M. J., & Blamire, A. M. (2010). Functional connectivity in late-life depression using resting-state functional magnetic resonance imaging. *The American Journal of Geriatric Psychiatry, 18*(7), 643–651.

Kim, M. J., Hamilton, J. P., & Gotlib, I. H. (2008). Reduced caudate gray matter volume in women with major depressive disorder. *Psychiatry Research: Neuroimaging, 164*(2), 114–122.

Krishnan, K. R. R., McDonald, W. M., Escalona, P. R., Doraiswamy, P. M., Na, C., Husain, M. M., … & Nemeroff, C. B. (1992). Magnetic resonance imaging of the caudate nuclei in depression: preliminary observations. *Archives of General Psychiatry, 49*(7), 553–557.

Lange, N., & Zeger, S. L. (1997). Non-linear Fourier Time Series Analysis for Human Brain Mapping by Functional Magnetic Resonance Imaging. *Journal of the Royal Statistical Society: Series C (Applied Statistics), 46*(1), 1–29.

Lin, C. F., & Zhu, J. D. (2012). Hilbert–Huang transformation-based time-frequency analysis methods in biomedical signal applications. *Proceedings of the Institution of Mechanical Engineers, Part H: Journal of Engineering in Medicine, 226*(3), 208–216.

Liu, C. H., Ma, X., Wu, X., Fan, T. T., Zhang, Y., Zhou, F. C., … & Zhang, D. (2013). Resting-state brain activity in major depressive disorder patients and their siblings. *Journal of Affective Disorders, 149*(1), 299–306.

Liu, F., Guo, W., Liu, L., Long, Z., Ma, C., Xue, Z., … & Du, H. (2013). Abnormal amplitude low-frequency oscillations in medication-naive, first-episode patients with major depressive disorder: a resting-state fMRI study. *Journal of Affective Disorders, 146*(3), 401–406.

Liu, J., Ren, L., Womer, F. Y., Wang, J., Fan, G., Jiang, W., … & Wang, F. (2014). Alterations in amplitude of low frequency fluctuation in treatment-naïve major depressive disorder measured with resting-state fMRI. *Human Brain Mapping, 35*(10), 4979–4988.

Liu, Z., Xu, C., Xu, Y., Wang, Y., Zhao, B., Lv, Y., … & Du, C. (2010). Decreased regional homogeneity in insula and cerebellum: a resting-state fMRI study in patients with major depression and subjects at high risk for major depression. *Psychiatry Research: Neuroimaging, 182*(3), 211–215.

Mah, L., Zarate, C. A., Singh, J., Duan, Y. F., Luckenbaugh, D. A., Manji, H. K., & Drevets, W. C. (2007). Regional cerebral glucose metabolic abnormalities in bipolar II depression. *Biological Psychiatry, 61*(6), 765–775.

Malykhin, N. V., & Coupland, N. J. (2015). Hippocampal neuroplasticity in major depressive disorder. *Neuroscience, 309*, 200–213.

Martis, R. J., Acharya, U. R., Tan, J. H., Petznick, A., Yanti, R., Chua, C. K., … & Tong, L. (2012). Application of empirical mode decomposition (EMD) for automated detection of epilepsy using EEG signals. *International Journal of Neural Systems, 22*(06), 1250027.

McIntyre, R. S., Harrison, J., Loft, H., Jacobson, W., & Olsen, C. K. (2016). The effects of vortioxetine on cognitive function in patients with major depressive disorder: a meta-analysis of three randomized controlled trials. *International Journal of Neuropsychopharmacology*, 19(10).

Mezer, A., Yovel, Y., Pasternak, O., Gorfine, T., & Assaf, Y. (2009). Cluster analysis of resting-state fMRI time series. *Neuroimage, 45*(4), 1117–1125.

Murray, E. A., Wise, S. P., & Drevets, W. C. (2011). Localization of dysfunction in major depressive disorder: prefrontal cortex and amygdala. *Biological Psychiatry, 69*(12), e43–e54.

Obuchowski, N. A. (2003). Receiver operating characteristic curves and their use in radiology. *Radiology, 229*(1), 3–8.

Otte, C., Gold, S. M., Penninx, B. W., et al. (2016). Major Depressive Disorder. *Nature Reviews Disease Primers, 2*,(16065).

Peng, Z. K., Peter, W. T., & Chu, F. L. (2005). A comparison study of improved Hilbert–Huang transform and wavelet transform: application to fault diagnosis for rolling bearing. *Mechanical Systems and Signal Processing, 19*(5), 974–988.

Pepe, M. S., Cai, T., & Longton, G. (2006). Combining predictors for classification using the area under the receiver operating characteristic curve. *Biometrics, 62*(1), 221–229.

Pepe, M. S., & Thompson, M. L. (2000). Combining diagnostic test results to increase accuracy. *Biostatistics, 1*(2), 123–140.

Pizzagalli, D. A., Holmes, A. J., Dillon, D. G., Goetz, E. L., Birk, J. L., Bogdan, R., … & Fava, M. (2009). Reduced caudate and nucleus accumbens response to rewards in unmedicated individuals with major depressive disorder. *American Journal of Psychiatry, 166*(6), 702–710.

Qian, L., Zhang, Y., Zheng, L., Fu, X., Liu, W., Shang, Y., … & Gao, J. H. (2017). Frequency specific brain networks in Parkinson's disease and comorbid depression. *Brain Imaging and Behavior, 11*(1), 224–239.

Qian, L., Zhang, Y., Zheng, L., Shang, Y., Gao, J. H., & Liu, Y. (2015). Frequency dependent topological patterns of resting-state brain networks. *PloS One*, 10(4), e0124681.

Qiu, Y. W., Han, L. J., Lv, X. F., Jiang, G. H., Tian, J. Z., Zhuo, F. Z., … & Zhang, X. L. (2011). Regional homogeneity changes in heroin-dependent individuals: resting-state functional MR imaging study. *Radiology, 261*(2), 551–559.

Rigucci, S., Serafini, G., Pompili, M., Kotzalidis, G. D., & Tatarelli, R. (2010). Anatomical and functional correlates in major depressive disorder: the contribution of neuroimaging studies. *The World Journal of Biological Psychiatry, 11*(2–2), 165–180.

Robertson, H. P. (1929). The uncertainty principle. *Physical Review, 34*(1), 163.

Sheline, Y. I. (2000). 3D MRI studies of neuroanatomic changes in unipolar major depression: the role of stress and medical comorbidity. *Biological Psychiatry, 48*(8), 791–800.

Sheline, Y. I. (2003). Neuroimaging studies of mood disorder effects on the brain. *Biological Psychiatry, 54*(3), 338–352.

Sheline, Y. I. (2011). Depression and the hippocampus: cause or effect? *Biological Psychiatry, 70*(4), 308.

Skidmore, F., Korenkevych, D., Liu, Y., He, G., Bullmore, E., & Pardalos, P. M. (2011). Connectivity brain networks based on wavelet correlation analysis in Parkinson fMRI data. *Neuroscience Letters, 499*(1), 47–51.

Song, X., Zhang, Y., & Liu, Y. (2014). Frequency specificity of regional homogeneity in the resting-state human brain. *PloS One*, 9(1), e86818.

Song, X., Zhou, S., Zhang, Y., Liu, Y., Zhu, H., & Gao, J. H. (2015). Frequency-dependent modulation of regional synchrony in the

human brain by eyes open and eyes closed resting-states. *PloS One*, 10(11), e0141507.

Surhone, L. M., Tennoe, M. T., Henssonow, S. F., & Cauchy, A. L. (2013). Cauchy Principal Value. *Betascript Publishing*.

Tahmasian, M., Knight, D. C., Manoliu, A., Schwerthöffer, D., Scherr, M., Meng, C., … & Drzezga, A. (2013). Aberrant intrinsic connectivity of hippocampus and amygdala overlap in the fronto-insular and dorsomedial-prefrontal cortex in major depressive disorder. *Frontiers in Human Neuroscience*, 7.

Tononi, G., McIntosh, A. R., Russell, D. P., & Edelman, G. M. (1998). Functional clustering: identifying strongly interactive brain regions in neuroimaging data. *Neuroimage, 7*(2), 133–149.

Tzourio-Mazoyer, N., Landeau, B., Papathanassiou, D., Crivello, F., Etard, O., Delcroix, N., … & Joliot, M. (2002). Automated anatomical labeling of activations in SPM using a macroscopic anatomical parcellation of the MNI MRI single-subject brain. *Neuroimage, 15*(1), 273–289.

Van De Ville, D., Blu, T., & Unser, M. (2006). Surfing the brain. *IEEE Engineering in Medicine and Biology Magazine, 25*(2), 65–78.

Van Someren, E. J. (2011). Slow brain oscillations of sleep, resting state and vigilance (Vol. 193). Elsevier.

Videbech, P. (2000). PET measurements of brain glucose metabolism and blood flow in major depressive disorder: a critical review. *Acta Psychiatrica Scandinavica, 101*(1), 11–20.

Wu, Q. Z., Li, D. M., Kuang, W. H., Zhang, T. J., Lui, S., Huang, X. Q., … & Gong, Q. Y. (2011). Abnormal regional spontaneous neural activity in treatment-refractory depression revealed by resting-state fMRI. *Human Brain Mapping, 32*(8), 1290–1299.

Xie, H., & Wang, Z. (2006). Mean frequency derived via Hilbert-Huang transform with application to fatigue EMG signal analysis. *Computer Methods and Programs in Biomedicine, 82*(2), 114–120.

Yang, H., Long, X. Y., Yang, Y., Yan, H., Zhu, C. Z., Zhou, X. P., … & Gong, Q. Y. (2007). Amplitude of low frequency fluctuation within visual areas revealed by resting-state functional MRI. *Neuroimage, 36*(1), 144–152.

Yao, Z., Wang, L., Lu, Q., Liu, H., & Teng, G. (2009). Regional homogeneity in depression and its relationship with separate depressive symptom clusters: a resting-state fMRI study. *Journal of Affective Disorders, 115*(3), 430–438.

Young, C. B., Chen, T., Nusslock, R., Keller, J., Schatzberg, A. F., & Menon, V. (2016). Anhedonia and general distress show dissociable ventromedial prefrontal cortex connectivity in major depressive disorder. *Translational Psychiatry*, 6(5), e810.

Yu-Feng, Z., Yong, H., Chao-Zhe, Z., Qing-Jiu, C., Man-Qiu, S., Meng, L., … & Yu-Feng, W. (2007). Altered baseline brain activity in children with ADHD revealed by resting-state functional MRI. *Brain and Development, 29*(2), 83–91.

Zeng, L. L., Shen, H., Liu, L., Wang, L., Li, B., Fang, P., … & Hu, D. (2012). Identifying major depression using whole-brain functional connectivity: a multivariate pattern analysis. *Brain, 135*(5), 1498–1507.

Zhou, Y., Yu, C., Zheng, H., Liu, Y., Song, M., Qin, W., … & Jiang, T. (2010). Increased neural resources recruitment in the intrinsic organization in major depression. *Journal of Affective Disorders, 121*(3), 220–230.

Zou, Q. H., Zhu, C. Z., Yang, Y., Zuo, X. N., Long, X. Y., Cao, Q. J., … & Zang, Y. F. (2008). An improved approach to detection of amplitude of low-frequency fluctuation (ALFF) for resting-state fMRI: fractional ALFF. *Journal of Neuroscience Methods, 172*(1), 137–141.

Zweig, M. H., & Campbell, G. (1993). Receiver-operating characteristic (ROC) plots: a fundamental evaluation tool in clinical medicine. *Clinical Chemistry, 39*(4), 561–577.